European Journal of Pharmaceutics and Biopharmaceutics 144 (2019) 193–206

Contents lists available at ScienceDirect

European Journal of Pharmaceutics and Biopharmaceutics

journal homepage: www.elsevier.com/locate/ejpb

4-Carboxyphenylboronic acid-decorated, redox-sensitive rod-shaped nano-micelles fabricated through co-assembling strategy for active targeting and synergistic co-delivery of camptothecin and gemcitabine

Yanyun Xu[a], Yushu Huang[a], Wei Lu[a], Shiyuan Liu[b], Yi Xiao[b,*], Jiahui Yu[a,*]

[a] Shanghai Engineering Research Center of Molecular Therapeutics and New Drug Development, School of Chemistry and Molecular Engineering, East China Normal University, Shanghai 200062, PR China

[b] Department of Radiology and Nuclear Medicine, Changzheng Hospital, Naval Medical University, Shanghai 200003, PR China

ARTICLE INFO

Keywords:
4-Carboxyphenylboronic acid
Redox-sensitive
Co-assembled rod-shaped nano-micelles
Synergistic co-delivery
Camptothecin
Gemcitabine

ABSTRACT

To achieve redox-controlled and tumor active targeting synergistic self-delivery of camptothecin and gemcitabine, redox-sensitive rod-shaped nano-micelles are fabricated through co-assembling between camptothecin-disulfide bond-PEG_{2000}-4-carboxyphenylboronic acid and camptothecin-disulfide bond-gemcitabine conjugate. Most of all, for multidrug resistant cancer cell line MCF-7/ADR which is more resistant against CPT, increasing content of CPT in the formulation is favorable for synergistic effect of CPT and GEM drug combination. Benefiting from simple co-assembling strategy, it is easy and convenient to adjust drug ratio of CPT/GEM to optimize the synergism of drug combination. In addition, nano-micelles fabricated from co-assembling are endowed with both high absolute drug concentration and enhanced colloidal stability, which is helpful to *in vivo* studies. Transmission electron microscopy observation confirmed the rod-shaped morphology, which is beneficial to cellular internalization, of co-assembled nano-micelles resulting from π-π stacking interactions of CPT moieties and appropriate hydrophilic and hydrophobic interactions during co-assembling. Taking advantages of the specific interactions between 4-carboxyphenylboronic acid and sialic acid, co-assembled nano-micelles exerted enhanced cellular internalization. Noteworthy, compared with cocktail mixture of free CPT and GEM, nano-micelles greatly alleviated drug reflux against MCF-7/ADR and 4T1 cells. The nano-micelles realized redox-controlled ratio-metric and synchronous delivery of CPT and GEM, thereby pronounced *in vitro* synergistic antiproliferative effect against MCF-7/ADR and 4T1cells. Furthermore, *in vivo* bio-distribution analysis indicated the preferential accumulation of nano-micelles at tumor site, which could increase therapeutic efficacy and decrease side effects of non-selective anticancer drugs. Taken together, the redox-sensitive CPBA decorated co-assembled nano-micelles provided a promising strategy for tumor active targeting and redox-controlled intracellular synergistic combinational delivery of chemotherapeutics.

1. Introduction

As one of mainstays for cancer treatments, combination chemotherapy has been adopted as standard to fight against variety of cancer types for a long time [1]. Benefiting from simultaneously modulating different signaling pathways, one of the prime advantages of combination chemotherapy is potential for providing synergism to maximize therapeutic effect thereby overcome dose-limiting toxicity

Abbreviations: ACN, Acetonitrile; ANOVA, Analysis of Variance; CAC, Critical Aggregation Concentration; CDI, 1,1′-Carbonyldiimidazle; CI, Combination Index; CPBA, 4-Carboxyphenylboronic Acid; CPT, Camptothecin; CPT-SS-GEM, Camptothecin-disulfide bond-gemcitabine conjugate; CPT-SS-OH, Camptothecin-2-Hydroxyethyl Disulfide Conjugate; CPT-SS-PEG-CPBA, Camptothecin-disulfide bond-PEG_{2000}-4-carboxyphenylboronic acid; DCM, Dichloromethane; DLS, Dynamic Light Scattering; DMSO, Dimethyl Sulfoxide; DRI, Dose Reduction Index; DTT, Dithiothreitol; EDCI, N-(3-dimethylaminopropyl)-N′-ethylcarbodiimide hydrochloride; Fa, Fraction Affected; FBS, Fetal Bovine Serum; GEM, Gemcitabine; GSH, Glutathione; IC_{50}, Half Maximal Inhibitory Concentration; MCF-7/ADR, Adriamycin Resistant Human Breast Cancer Cell Line; MDR, Multidrug Resistance; MTT, 3-(4,5-Dimethylthiazol-2-yl)-2, 5-diphenyltetrazolium Bromide; MWCO, Molecular Weight Cut Off; NHS, N-Hydroxysuccinimide; OD, Optical Density; PBA, Phenylboronic Acid; PBS, Phosphate Buffered Saline; PDI, Polydispersity Index; PEG_{2000}, Poly (ethylene glycol) (Molecular Weight 2000); P-gp, P-glycoprotein; RPMI-1640, Roswell Park Memorial Institute-1640 Culture Medium; SD, Standard Deviation; TEM, Transmission Electron Microscopy; THF, Tetrahydrofuran; 4T1, Marine Breast Cancer Cell Line

* Corresponding authors.
E-mail addresses: xiaoyi@188.com (Y. Xiao), jhyu@sist.ecnu.edu.cn (J. Yu).

https://doi.org/10.1016/j.ejpb.2019.09.019
Received 9 June 2019; Received in revised form 16 September 2019; Accepted 23 September 2019
Available online 24 September 2019
0939-6411/

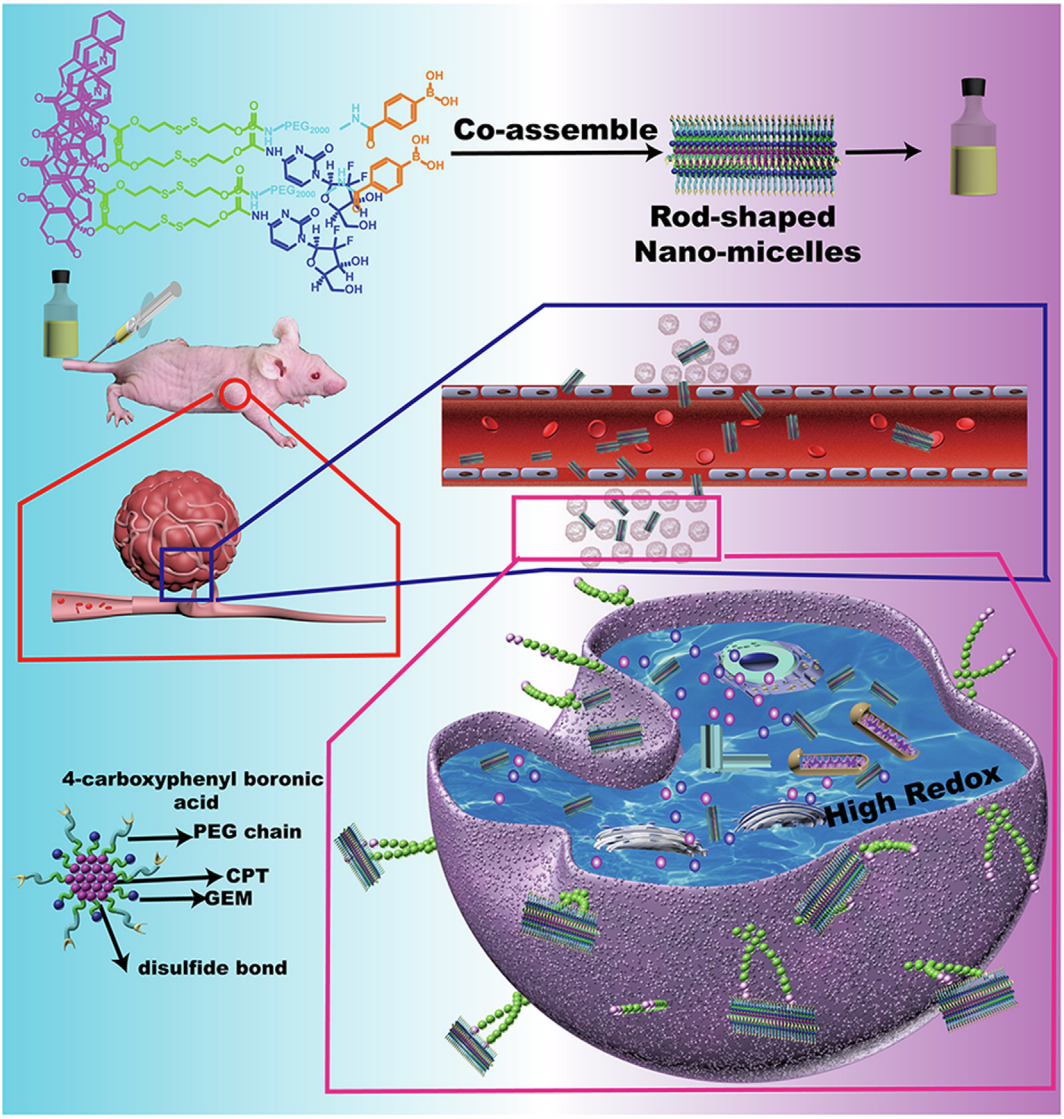

Fig.1. Graphic illustration of active targeting and redox-controlled synergistic co-delivery of camptothecin and gemcitabine achieved by CPBA decorated rod-shaped nano-micelles fabricated through simple co-assembling between CPT-SS-GEM and CPT-SS-PEG_{2000}-CPBA.

and deter development of drug resistance associated with cancer treatments [2]. Nevertheless, triumph of current combination chemotherapy is greatly hampered by administration of cocktail mixture of free drugs [3]. Upon systemic administration, drugs undergo distinctive physiological fates, non-uniform distribution and non-synchronous access to tumor tissues, which separates *in vitro* success from impressive clinical outcomes of cocktail combination therapy [4]. Taken together, it is imperative to develop drug delivery systems to mitigate the difficulties associated with conventional cocktail combination chemotherapy. Different from traditional cocktail administration, combinational therapies based on nano-drug delivery systems hold intriguing advantages, including uniform and concurrent delivery of drug combinations, maintaining the synergistic drug ratios, and controlling drug exposure sequences [5], therefore it is considered as an alternative approach for treatment of cancer in near future.

Moreover, as an inspiring strategy, drug self-delivery systems, consisted of active drugs or prodrugs, exhibit not only nanoscale characteristics but also controlled drug delivery by themselves without additional assistances. The prosperity of drug self-delivery systems could address the troublesome issues of traditional nano-carriers applied for combinational drug delivery, taking the metabolites of materials and the rather low drug loading capacity (typically lower than 10%) for instance [6].The frontier researches of drug self-delivery systems have gained increasing attention in recent years [7–10].

Inspired by pioneer's work, a carrier-free and redox-sensitive Janus nano-prodrug with pretty high drug loading capacity, camptothecin-disulfide bond-gemcitabine conjugate (CPT-SS-GEM), is fabricated and evaluated in our group [11]. Consisting of active drugs with different mechanisms of action, CPT-SS-GEM exhibits prominent synergistic antiproliferative efficacy in multiple cancer cell lines. Unfortunately, as drug concentration increasing, CPT-SS-GEM tended to self-assemble into nanofibers as exhibited in Fig S1A. Moreover, the formulation precipitate easily (Fig.S1B) due to the strong π-π stacking interactions among the camptothecin (CPT) moieties. As a result, the poor colloidal stability, aggregation formation and low absolute drug concentration come as major problems for its applications. Additionally, lack of specific active tumor targeting is another critical challenge for the CPT-SS-GEM self-assembled nano-prodrug.

Recently, it has been reported that alterations in sialylation regulate development and progression of cancers, including invasiveness and metastasis [12]. As a distinctive feature associated with malignant properties, abnormal sialylation in cancer cells serves as an important biomarker and provides a specific target for therapeutic intervention [13,14]. The alterations in sialylation is involved in several types of

cancers, like pancreas [15], stomach [16], colorectum [17], breast [18], bladder [19] and ovary [20]. It has been reported that phenylboronic acid (PBA) and its derivatives could selectively recognize the sialic acid on membranes of cancer cells [21]. In this context, functionalization of nano-drug delivery systems with PBA and its derivatives could be taken as a potential strategy for tumor-targeted delivery of genes and drugs [22,23].

Encouragingly, in recent years, numbers of studies have demonstrated that rod-shaped nanoparticles exerted enhanced cellular uptake and thereby improved drug delivery efficiency [24–27]. It is conceptually acknowledged that nanodrugs with elongated shape could provide more interactions between the multivalent targeting ligands and multivalent receptors on cell surface than those with spherical shape [28,29].

Moreover, nanodrugs with surface PEGylation could be conferred with long-circulating ability and well dispersity and stability in physiological environment.

Motivated by the crucial role of shape design in the process of drug delivery, here, we report the 4-carboxyphenylboronic acid (CPBA) decorated rod-shaped nano-micelles for active targeting and synergistic combinational self-delivery of CPT and GEM. To fabricate the co-assembled nano-micelles, camptothecin-disulfide bond-PEG_{2000}-4-carboxyphenylboronic acid (CPT-SS-PEG_{2000}-CPBA), an active targeting and redox-sensitive PEGylation prodrug of CPT, is applied to co-assemble with CPT-SS-GEM. CPBA, which can specifically recognize sialic acid is attached to PEG chain as an active targeting ligand as illustrated in Fig. 1.

An ideal drug delivery system for cancer treatment could realize trigger-responsive drug release, especially those cancer specific triggers [30]. Different triggers, such as pH, elevated temperature, redox, enzyme, external stimuli and combination of multiple triggers, have been applied to develop trigger-responsive drug delivery systems to maximize treatment efficacy. Among the various triggers, tumor intracellular high redox microenvironment is considered as an ideal trigger condition for pro-drug design. It is widely reported that, glutathione (GSH), a thiol-containing tripeptide capable of reducing disulfide bonds, is abundant in the cytoplasm of the cell (2–10 mM) [31], whereas it is rarely present in blood plasma (~20 μM) [32]. Moreover, the GSH concentration in some cancers is found to be about seven times higher than that in normal cells [33,34], which contributes to the high redox tumor microenvironment contrast to normal tissues and blood plasma. The higher concentrations of GSH in tumor cells can trigger release of drugs at the target site. The prodrug compounds containing simple disulfide bond or thioester can be efficiently cleaved by intracellular thiols [35,36] or reductase [37] while they are inert to many other chemical functional groups as well as reactions, making it easy for the synthesis and chemical modification of disulfide containing prodrugs. It is worth mentioning that both CPT-SS-PEG_{2000}-CPBA and CPT-SS-GEM are redox-sensitive prodrugs could be degraded in high redox tumor microenvironment. Under this condition, the co-assembled nano-micelles could realize self-delivery of two drugs with different mechanisms without the help of other excipients. Another merit of the simple co-assembling strategy is that it is convenient to increase the content of CPT in the formulation through adjusting ratio of the two redox-sensitive prodrug components. This property is beneficial for optimizing the synergism of nano-micelles against MCF-7/ADR cells which is more resistant against CPT. In addition, as expected, by using CPT-SS-PEG_{2000}-CPBA in the co-assemble process, not only the absolute drug concentration could be remarkably increased but also the colloidal stability could be greatly enhanced for the constructed co-assembled nano-micelles. Co-assembled nano-micelles remained uniform without cluster and bulk aggregates formation. Interestingly, the co-assembled nano-micelles showed rod-shaped morphology due to the balance of multiple interactions, including π-π stacking interactions of CPT moieties, hydrophilic and hydrophobic interactions. *In vitro* drug release studies verified the redox-triggered ratio-metric and synchronous rapid release of CPT and GEM from co-assembled nano-micelles. Moreover, the CPBA decorated co-assembled nano-micelles exerted obviously enhanced cellular internalization while cellular uptake against cells pretreated by free CPBA remarkably decreased. The aforementioned results demonstrated the sialic acid-mediated active targeting capacity of co-assembled nano-micelles. Noteworthy, compared with cocktail mixture of CPT and GEM, co-assembled nano-micelles not only greatly reduced drug reflux but also exhibited profound synergistic antiproliferative effect against MCF-7/ADR and 4T1 cells. Especially for MCF-7/ADR cells, co-assembled nano-micelles showed much lower IC_{50} value than other formulations. Additionally, *in vivo* bio-distribution analysis demonstrated that co-assembled nano-micelles preferentially accumulated at tumor site, which could decrease side effects and increase therapeutic efficacy of drugs.

2. Experimental section

2.1. Materials, cell culture and animals

Camptothecin, 4-carboxyphenylboronic acid, pinacol, *N*-Hydroxysuccinimide (NHS), *N*-(3-dimethylaminopropyl)-*N*′-ethylcarbodiimide hydrochloride (EDCI), and 1,1′-carbonyldiimidazle (CDI) are purchased from J&K Chemical Ltd. (Shanghai, China). Poly (ethylene glycol)$_{2000}$ (PEG_{2000}), 3-(4, 5-Dimethylthiazol-2-yl)-2, 5-diphenyltetrazolium bromide (MTT) are purchased from Sigma-Aldrich (Shanghai, China). NH_2-PEG_{2000}-NH_2 is kind gift from associated professor Yu Luo at East China Normal University. Culture medium RPMI 1640 is obtained from Gibco BRL. (Paris, France). Fetal bovine serum (FBS) and penicillin-streptomycin are obtained from HyClone (Logan, Utah, USA). Other chemicals are obtained from Sinopharm Chemical Reagent Co., Ltd. (Huangpu, Shanghai, China). Dichloromethane (DCM) is dried by refluxing over fresh CaH_2, and subsequent distilled before use. Tetrahydrofuran (THF) is dried by refluxing against fresh sodium, and subsequent distilled prior to use.

Marine breast cancer cell line 4T1 and multidrug resistant (MDR) human breast cancer cell subline MCF-7/ADR are obtained from cell bank of Chinese Academy of Sciences (Shanghai, China), and cultured in RPMI-1640 medium supplemented with 10% FBS and 1% penicillin and streptomycin under a humidified atmosphere containing 5% CO_2.

Female BABL/c nude mice (4–6 weeks old) are supplied by Shanghai Laboratory Animal Center, Chinese Academy of Sciences. Animals are maintained at animal care facility with free access to standard food and water under specific pathogen-free condition with temperature of 20-24 °C, relative humidity of 40-70%, and 12/12 h light-dark cycle in the Animal Laboratory Center of East China Normal University. Prior to the experiments, the animals are acclimatized for at least 7 days. All of animal experiments are carried out in accordance with guidelines of the Animal Ethics Committee of East China Normal University.

2.2. Instruments and measurements

^{1}H NMR were recorded on a Bruker Avarice ™ 400 NMR spectrometer. A Malvern Zetasizer apparatus equipped with a 4.0 mW He-Ne laser (Malvern Instruments, UK) was applied to perform dynamic light scattering (DLS) measurements. All samples were analyzed at a scattering angle of 90° and λ = 633 nm. The observation of morphology was performed by transmission electron microscopy (TEM) with JEOL 2100 instrument at 120 kV. An Agilent 1200 (Agilent Technologies INc., Shanghai Branch) with a Zorbax Eclipse XDB-C_{18} column (5 μm, 4.6 mm × 250 mm) at 30 °C was applied to conduct Reversed Phase High Performance Liquid Chromatography (RP-HPLC) analysis. The UV–vis spectra measurements were performed by UV-1800 UV spectrophotometer (Shimadzu Corp., Japan).

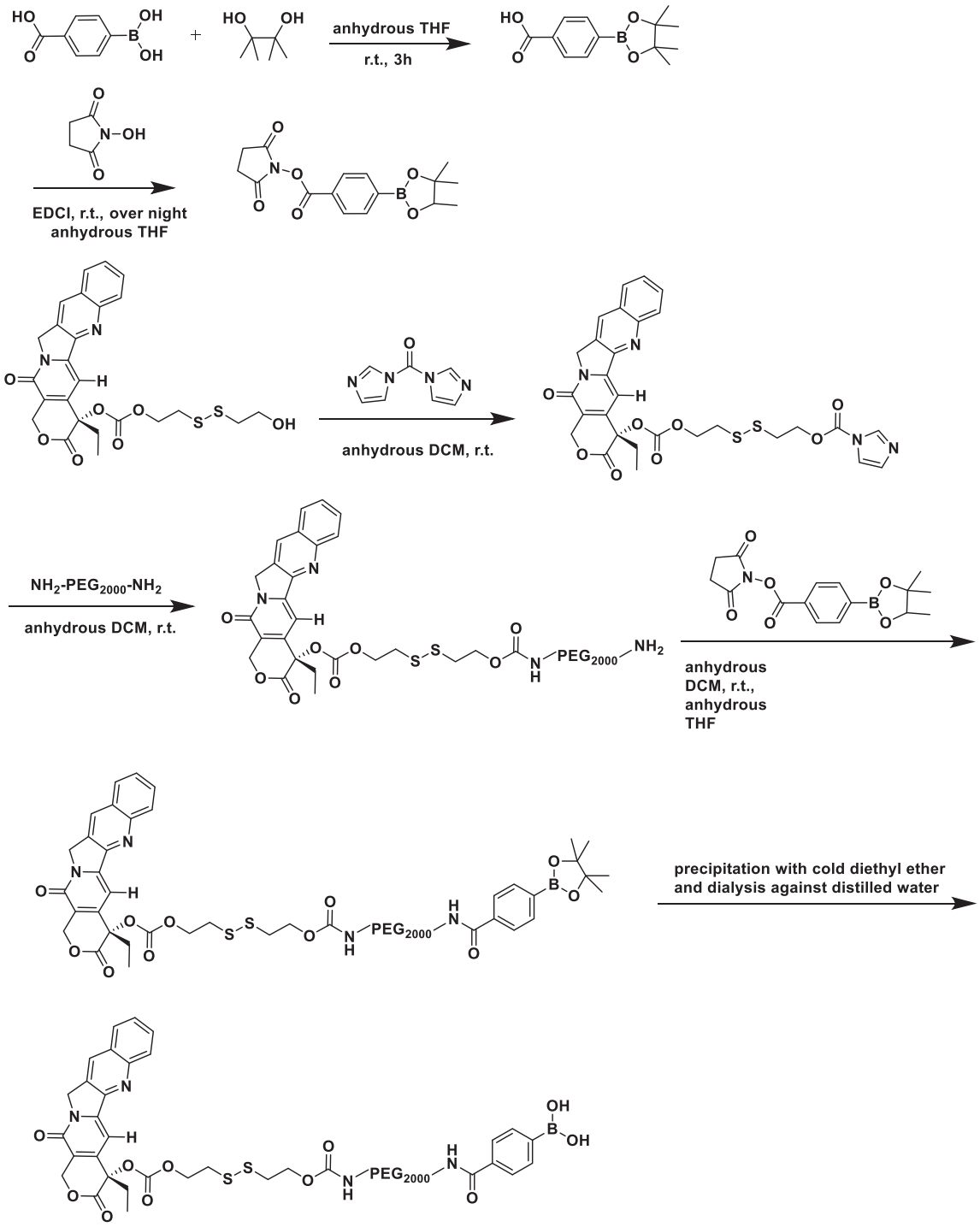

Scheme 1. Synthesis route of CPT-SS-PEG_{2000}-CPBA.

2.3. Synthesis

CPT-SS-OH and CPT-SS-GEM were synthesized as described in our previous published literature [11]. CPT-SS-PEG_{2000}-CPBA was synthesized in process described in Electronic Supplementary Information. The synthesis route is presented in Scheme 1.

2.4. Determination of critical aggregation concentration (CAC)

DLS was applied to evaluate CAC of CPT-SS-PEG_{2000}-CPBA according to the method previously reported [38]. Solutions of CPT-SS-PEG_{2000}-CPBA with different concentrations (1×10^{-5} to 0.7 mg/mL) were prepared and analyzed. Based on intensity of scattering light versus log concentration curve, CAC was determined as the intersection point through extrapolating intensity of scattering light at low and high concentration ranges. The measurements were performed in triplicate.

2.5. Fabrication and characterization of the co-assembled nano-formulation

Solvent evaporation method was applied to fabricate co-assembled nano-formulation. Briefly, CPT-SS-GEM (8 mg) and CPT-SS-PEG_{2000}-CPBA (80 mg) are dissolved in THF (1 mL) through sonication. The resulting solution was kept stirring for 30 min at room temperature. Subsequently, under continuous vigorous stirring, the THF solution was

added dropwise into ultrapure water (9 mL) prepared from a Milli-Q system (Merck Millipore, Tokyo, Japan). In order to evaporate organic solvent, the mixture was stirred for another 24 h at room temperature. The co-assembled nano-formulation was obtained after complete evaporation of THF.

The physicochemical properties of co-assembled nano-formulation were characterized, including size, zeta potential, morphology and colloidal stability. Particle size was statistically analysis through TEM images, and zeta potential was determined in triplicate by DLS. Specimens for TEM observation were prepared by carefully depositing a drop of co-assembled nano-formulation onto a carbon film coated copper grid (300 mesh). After dried at room temperature, the grids were observed by TEM to capture morphology of co-assembled nano-formulation.

In order to evaluate the time-dependent stability of co-assembled nano-formulation against phosphate buffered solution (PBS) under storage condition, the freshly prepared co-assembled nano-formulation was dispersed in 10 mM pH 7.4 PBS with concentration of 1 mg/mL and maintained at 4 °C. The size and size distribution of the dispersion were periodically measured by DLS. The measurements were performed for three times and data were expressed as mean ± SD.

Meanwhile, in drug delivery, it is an important issue for nano-drugs to maintain their stability after intravenous injection. The protein adsorption in plasma may result in aggregation, precipitation or disassembly of nano-drugs, which could decrease the therapeutic efficacy. To gain further insights into protein adsorption and the stability, the CPBA decorated co-assembled nano-micelles were incubated with bovine serum albumin (BSA, 500 μM) for different times (12, 24, 48 and 72 h). Then, the change of particle size at different times of incubation with BSA was assessed using fluorescence correlation spectroscopy (FCS), as FCS is a very sensitive method to determine the drug-protein interaction. The principle of FCS is based on the measurement of the change in characteristic diffusion time (τ_D) of FITC labeled CPBA decorated co-assembled nano-micelles as the characteristic diffusion time is related to the size of the nano-micelles. The preparation of FITC labeled CPBA decorated co-assembled nano-micelles and the FCS setup were described in Electronic Supplementary Information.

2.6. In vitro reduction-triggered drug release

Reduction-triggered drug-release profile of co-assembled nano-formulation was performed by dialysis method. Quantitatively analysis of drug release was conducted by RP-HPLC.

In detail, 2 mL suspension of co-assembled nano-micelles (50 μM equivalent to CPT) in 10 mM PBS with different pH values (pH 5.0, 6.5, 7.4) and presence of 2 mM or 20 μM dithiothreitol (DTT) was enclosed in a dialysis bag (MWCO: 1000 Da). The dialysis bag of specific condition was immersed in the relevant dispersion medium. Then, all of dialysis bags were maintained at 37 °C and 100 rpm in a THZ-C isothermal shaker. At designated time points, 200 μL of dispersion was withdrawn and replaced with equal volume of fresh release medium. Then, phosphoric acid (85%, 30 μL) was added to terminate drug release process. Subsequently, all of the samples were diluted with methanol (chromatographically pure, 170 μL) prior to RP-HPLC measurement. For RP-HPLC analysis, components of solvent system and gradient were set as stated following: solvent A (acetonitrile, ACN), solvent B (water, containing 0.1% trifluoroacetic acid, TFA), 95–5% solvent A in 0–9 min (liner), 5% solvent A in 9–14 min (isocratic), 5% solvent A in 14–14.5 min (isocratic), 5–95% solvent A in14.5–20 min (liner), 1 mL/min. To simultaneous analysis of CPT and GEM, the Agilent 1200 UV/vis detector was set at 254 nm. The amount of released CPT and GEM was calculated by calibration curve of native CPT and GEM. Analysis was performed in triplicates, and data were expressed as mean ± SD.

2.7. In vitro cellular internalization

The MCF-7/ADR and 4T1 cells, 2.0×10^5 cells per well, were seeded in 6-well plates and incubated for 24 h. Thereafter, culture media were replaced with 2 mL of fresh media containing CPT (50 μM), GEM (12.5 μM), cocktail mixture of CPT and GEM (molar ratio of CPT to GEM: 4/1) and co-assembled nano-micelles (50 μM equivalent to CPT), and cells were cultured for another 4 h or 24 h, respectively. Subsequently, cells were washed with cold PBS for three times after removal of culture medium. Then, cells were fixed with 4% paraformaldehyde for 0.5 h at 25 °C. Then, cells were washed with PBS for three times and DiI with working concentration of 10 μM was added to stain cells for 15 min at 37 °C Finally, cells were washed with PBS for three times and fluorescence images were captured by an inverted fluorescence microscope (Olympus, TH4-200 with Olympus UHGLGPS).

Additionally, for competitive assay, cells were incubated with free CPBA (5 mM) for 30 min before treatment with CPT, GEM, cocktail mixture of CPT and GEM and co-assembled nano-micelles. Moreover, in order to verify cellular internalization of co-assembled nano-micelles is energy-dependent, cells were kept at 4 °C for 4 h in fridge for low temperature treatment.

Before the competitive assay of *in vitro* cellular internalization, control cytotoxicity studies of both 5 mM CPBA pretreatment + CPT and 5 mM CPBA were carried out. In detail, for 5 mM CPBA pretreatment + CPT, 1×10^4 cells in 200 μL culture medium were seeded in 96-well plates. After incubated for 24 h, culture media were replaced with the 200 μL culture medium containing 5 mM CPBA and the cells were incubated for 30 min. Subsequently, each well was washed by 200 μL PBS for three times. The 200 μL culture medium containing CPT of different concentrations was added and the cells were cultured for another 72 h. Then, 20 μL MTT stock solution (5 mg/mL) was added. Subsequently, culture medium was removed carefully after incubation for additional 4 h. Then, the obtained blue formazan was dissolved by DMSO (100 μL), and plates were measured at 550 nm with an automatic BIO-TEK microplate reader (Powerwave XS, USA). After subtraction optical density (OD) of blank control, the measured OD values were applied to calculate cell viability expressed as percentage of negative control. The experiment was conducted in triplicate and data were expressed as mean ± SD.

For cytotoxicity of CPBA, 5×10^4 cells in 200 μL culture medium were seeded in 96-well plates. After incubated for 24 h, culture media were replaced with the 200 μL culture medium containing different concentration of CPBA and the cells were incubated for 30 min. Subsequently, 20 μL MTT stock solution (5 mg/mL) was added. Then, culture medium was removed carefully after incubation for additional 4 h. The obtained blue formazan was dissolved by 100 μL DMSO and the plates were measured at 550 nm with an automatic BIO-TEK microplate reader (Powerwave XS, USA). After subtraction optical density (OD) of the blank control, the measured OD values were applied to calculate cell viability expressed as percentage of negative control. The experiment was conducted for three times and data were expressed as mean ± SD.

For quantitative determination of cellular internalization, after the last washing of cells with cold PBS, cells were trypsined and collected from the wells, and transferred into a polypropylene centrifuge tube (15 mL). Subsequently, cell suspension was sonicated, 10 s intervals followed by 20 s pulses for 10 min at 0 °C (ultrasonicator probe, Vibra cell 750). Subsequently, after centrifugation of cell suspension (1500 rpm) for 10 min at 4 °C, supernatant was collected and lyophilized. After the prepared samples dissolved in acetonitrile and centrifuged at 5000 rpm for 5 min, supernatant of the obtained sample was analyzed by RP-HPLC.

2.8. Drug accumulation and reflux

For investigation of drug accumulation and reflux, 1.0×10^5 cells

per well of two cell lines, MCF-7/ADR and 4T1, were seeded into 12-well plates. After incubation for 24 h, CPT, GEM, cocktail mixture of CPT and GEM, co-assembled nano-micelles (100 μM equivalent to CPT) were added to the wells and incubated with cells for 4 h at 37 °C. For blank control, cells were treated with culture medium without drugs. Drugs retained in culture medium were quantified through fluorescence intensity of CPT with excitation at 360 nm and emission at 450 nm with an automatic BIO-TEK microplate reader (Powerwave XS, USA).

Subsequently, culture media were removed and cells were carefully washed with PBS for three times. Then, fresh culture medium was added into each well, and cells were incubated for another 1 h or 4 h. At desired time point, culture medium from each well were collected for fluorescence measurement (excitation at 360 nm and emission at 450 nm) with an automatic BIO-TEK microplate reader (Powerwave XS, USA). The amount of drug accumulation or reflux was calculated through standard curve of CPT. The experiment was carried out in triplicate and data were expressed as mean ± SD.

2.9. In vitro cytotoxicity

The cytotoxicity against MCF-7/ADR and 4T1cells were evaluated by standard MTT assay. In detail, 5×10^3 cells in 200 μL culture medium were seeded in 96-well plates. After incubated for 24 h, culture media were replaced with serial dilutions of co-assembled nano-micelles, cocktail mixture of CPT and GEM, free CPT and free GEM in 200 μL fresh culture medium. The drug concentration was equivalent to molarity of free CPT. As negative control, cells were treated with culture medium without drugs. After another desired period of incubation, 20 μL MTT stock solution (5 mg/mL) was added. Subsequently, culture medium was removed carefully after incubation for additional 4 h. Then, the obtained blue formazan was dissolved by DMSO (100 μL), then plates were measured at 550 nm with an automatic BIO-TEK microplate reader (Powerwave XS, USA). After subtraction optical density (OD) of blank control, the measured OD values were applied to calculate cell viability expressed as percentage of negative control. The experiment was conducted in triplicate and data were expressed as mean ± SD.

2.10. Determination of synergistic effect

Combination Index (CI) calculated by Chou-Talalay method [39,40] was applied to quantify the nature and extent of drug interactions. Combination index is defined as:

$$\text{Combination Index (CI)} = \frac{D_1}{D_{x1}} + \frac{D_2}{D_{x2}} \quad (1)$$

Dx_1 and Dx_2 respectively represents dose for drug 1 and drug 2 used alone to achieve particular drug effect level (e.g., 50% inhibition of cell viability). D_1 and D_2 represent dose of drug 1 and drug 2 in drug combinations to achieve the same drug effect level. CI value, plotted against drug effect level, lower than 1, equal to 1, or higher than 1 represents synergism, additivity and antagonism, respectively.

Moreover, Dose Reduction Index (DRI) values were also calculated. As another important parameter of drug combination, DRI values quantify the reduced folds of each drug dose in synergistic combination comparing with dose of each drug used alone at a given drug effect level. It is widely acknowledged that dose reduction of drug combinations leads to retained therapeutic efficacy while reduced toxicity toward the host.

2.11. In vivo biodistribution

For biodistribution analysis, tumor model was established by subcutaneously injection of about 1.0×10^6 4T1 cells into right upper armpit of female BABL/c nude mice (4–6 weeks old, weighting approximately 20 g). When tumor volumes reached about 400–500 mm^3, the tumor-bearing mice were randomly divided into four groups (n = 3) and intravenously administrated with co-assemble nano-micelles, cocktail mixture of CPT and GEM, free CPT and free GEM at a dose of 5 mg CPT/kg body weight per mouse. The mice were executed post administration for 24 h. Tumors and main organs, including heart, liver, spleen, lung and kidney were excised carefully and washed with saline, weighed after drying, and homogenized in 1 mL mixture of water and DMSO (V/V: 1/1). The mixture was vortexed for 5 min and centrifuged at 10,000*g* for 15 min. Then, the supernatant fractions were collected, and content of CPT in each sample was analyzed based on fluorescence emission intensity of CPT at 450 nm and excitation at 360 nm with fluorescent automatic BIO-TEK microplate reader (Powerwave XS, USA). The results were normalized with organ or tumor weights in the corresponding samples.

2.12. Statistical analysis

Unless otherwise mentioned, data were presented as means ± SD. For two groups, data were analyzed by two-tailed Student's t-tests. For multiple groups, data were analyzed by One-way ANOVA followed by Turkey post-tests. Bonferroni's multiple comparison post-tests were applied to determine significance between specific groups. Possibilities less than 0.05 was considered significant and significant levels were expressed as $^*p < 0.05$, $^{**}p < 0.01$, $^{***}p < 0.001$.

3. Results and discussion

3.1. Synthesis and characterization of CPT-SS-PEG_{2000}-CPBA

Scheme 1 depicted schematic illustration of synthesis procedure of CPT-SS-PEG_{2000}-CPBA. Firstly, the hydroxyl group of CPT-SS-OH was modified with CDI coupling agent for conjugation with primary amino group of NH_2-PEG_{2000}-NH_2 to obtain CPT-SS-PEG_{2000}-NH_2. Secondly, carboxyl group of pinacol protected 4-caroxyphenylboronic acid was activated with NHS/EDCI for subsequent conjugation with CPT-SS-PEG_{2000}-NH_2. Treated by precipitation, dialysis and lyophilization, CPT-SS-PEG_{2000}-CPBA was obtained as pale yellow solid. The build-in disulfide bond endowed CPT-SS-PEG_{2000}-CPBA with redox-sensitivity. The obtained product was characterized by ^{1}H NMR.

Figs. S2–S7 respectively represents ^{1}H NMR of CPBA, pinacol-CPBA, pinacol-CPBA-NHS, CPT-SS-OH, CPT-SS-PEG_{2000}-NH_2 and CPT-SS-PEG_{2000}-CPBA. As shown in ^{1}H NMR of CPT-SS-OH and CPT-SS-PEG_{2000}-NH_2, the disappearance of proton signal at 4.81–4.84 ppm ascribed to hydroxyl group of CPT-SS-OH and the existence of characteristic protons signals of PEG chain at 3.50–3.56 ppm in Fig. S6 verify the successful synthesis of CPT-SS-PEG_{2000}-NH_2. In addition, integration ratio at 0.91–0.94 ppm (10, methyl protons of CPT moiety) and 3.50–3.56 ppm (protons of PEG chain) confirmed the 1:1 conjugation of CPT-SS-OH and NH_2-PEG2000-NH_2. Furthermore, as presented in Fig. S7, characteristic proton signal of CPBA at 7.71–7.90 ppm proves the decoration of CPBA on PEG chain. In a word, the aforementioned results demonstrate the successful synthesis of CPT-SS-PEG_{2000}-CPBA.

3.2. Fabrication and characterization of the co-assembled nano-formulation

3.2.1. Critical aggregation concentration (CAC) value of CPT-SS-PEG_{2000}-CPBA

CAC value of CPT-SS-PEG_{2000}-CPBA was determined by DLS through the abrupt change of scattering light intensity due to nanoparticles formation. As shown in Fig. S8, intensities of scattering light of CPT-SS-PEG_{2000}-CPBA at concentrations lower than CAC are approximately constant and similar as that of deionized water. As the concentration of CPT-SS-PEG_{2000}-CPBA increasing, scattering light intensity displayed linear increment due to formation of nanoparticles. The CAC is ca 0.02 mg/mL determined as the intersection point through

extrapolating the scattering light intensity versus log concentration curve at low and high concentration ranges. It is supposed that the proper CAC of CPT-SS-PEG$_{2000}$-CPBA could contribute to retain high colloidal stability of co-assembled nano-formulation.

3.2.2. Size, zeta potential and morphology

Benefiting from amphipathy of both CPT-SS-GEM and CPT-SS-PEG$_{2000}$-CPBA as well as the same CPT moiety of the two molecules, the co-assembling strategy was conducted successfully. In order to obtain co-assembled formulation with both good colloidal stability and increased absolute drug concentration as well as better synergism of CPT and GEM drug combination against MCF-7/ADR cells, the co-assemble was carried out at 4/1 M ratio of CPT/GEM (molar ratio of CPT-SS-PEG$_{2000}$-CPBA/CPT-SS-GEM is 3/1) based on the exploration of co-assemble at different molar ratios of CPT-SS-PEG$_{2000}$-CPBA/CPT-SS-GEM and cytotoxicity of cocktail mixture of CPT and GEM at different CPT/GEM molar ratios. Aqueous co-assembled nano-formulation was obtained as pale-yellow suspension (Fig. S9).

For the rod-shaped nanoparticles, which are different from the rather perfect spherical particles, the size measurements by DLS are not very meaningful, here the particle size was obtained by statistical analysis of TEM images. As shown in Fig. 2A, TEM observation reveals that the prepared samples display as rod-shaped nano-micelles with an average length of ca. 400–500 nm and aspect ratio of 2.23 ± 0.37 (n = 524, some TEM images have been presented as supplement in Fig. S17).

Meanwhile, zeta potential of co-assembled nano-formulation in ultrapure water was measured by DLS as 4.64 ± 0.59 mV presented in Fig. S10.

Additionally, in order to gain insight into the underlying mechanism of formation of rod-shaped nano-micelles, interactions between the two molecules, CPT-SS-PEG$_{2000}$-CPBA and CPT-SS-GEM, were investigated through UV–vis absorption spectra. The UV–vis spectra of mixture of CPT-SS-PEG$_{2000}$-CPBA (10 μg/mL) and CPT-SS-GEM (1 μg/mL) in THF and co-assembled nano-micelles in water (10 μg/mL CPT-SS-PEG$_{2000}$-CPBA and 1 μg/mL CPT-SS-GEM) were measured with a UV-1800 UV spectrophotometer. Fig. 2B displayed the UV–vis absorption spectra of co-assembled nano-micelles suspension in water and the mixture solution of CPT-SS-PEG$_{2000}$-CPBA and CPT-SS-GEM in anhydrous THF, respectively.

UV–vis spectrum of the mixture solution in anhydrous THF where molecules are considered to exist in free molecules without aggregated state (Fig. 2B), displayed two conspicuous absorption peaks at 364 nm and 378 nm. In contrast, for co-assembled nano-micelles dispersed in water, the inferior absorption intensity and remarkable blue shift of the two main peaks at 351 nm and 362 nm indicate formation of *J*-aggregated π-π stacking of CPT chromophores in rod-shaped co-assembled nano- micelles [41,42]. It is supposed that the inferior absorption intensity and remarkable blue shift are related to the following two reasons. One is that the formation of π-π stacking always promote the interactions between the π-bonding orbital and the π* anti-bonding orbital, which further reduce the energy of π-orbital and increase the energy of π* orbital as well as weaken the conjugation effect. Then the absorption peaks shift to a shorter wavelength and the peak intensity

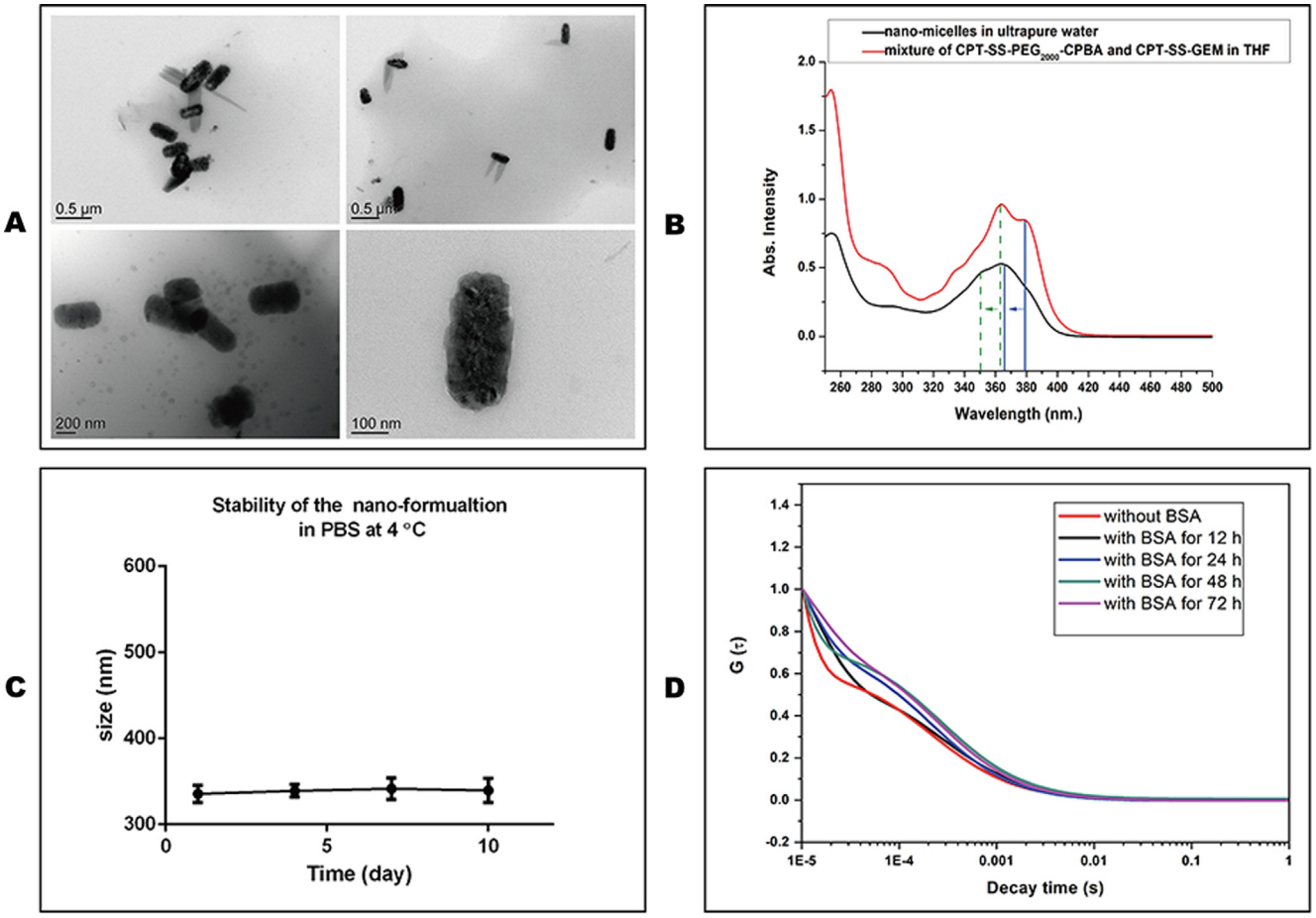

Fig. 2. Characterization of co-assembled nano-formulation. (A) The rod-shaped morphology of co-assembled nano-formulation confirmed by TEM (B) UV–vis absorption spectrum of co-assembled nano-micelles in water and mixture of CPT-SS-PEG$_{2000}$-CPBA and CPT-SS-GEM in THF (C) Size variation of co-assembled nano-formulation in 10 mM pH 7.4 PBS at 4 °C for 10 days determined by DLS (D) Size variation of co-assembled nano-formulation incubated with 500 μM BSA for different times at 37 °C determined by FCS.

decreased. The other reason is the formation of nano-micelles which makes the structure denser and the CPT moieties encapsulated in the hydrophobic core, resulting in a decrease in peak intensity.

3.2.3. Time-dependent stability of co-assembled nano-micelles in PBS

The time-dependent stability of co-assembled nano-micelles in PBS was determined by DLS based on measurement of sizes variation. As presented in Fig. 2C, hydrodynamic sizes of co-assembled nano-micelles did not change significantly within a period of 10 days, suggesting the good stability of the co-assembled nano-micelles under physiological pH of 7.4 at storage condition.

3.2.4. Protein adsorption of co-assembled nano-micelles

The stability of nano-drugs after intravenous injection is an important issue for effective drug delivery. Because the protein adsorption of nano-drugs might result in the agglomeration of the nano-drugs, which in turn hamper the drug delivery and therapeutic efficacy. In this context, the FITC-labeled CPBA decorated co-assembled nano-micelles were incubated 500 μM BSA for different times and the change of particle size was assessed using FCS. Fig. 2D showed the normalized autocorrelation curves. As presented, compared with that of the control (without BSA), during the first 12 h of incubation with BSA, particle size of the co-assembled nano-micelles showed minimal change (slightly increased). However, the correlation curves shifted to the right as the incubation period increased to 24, 48 and 72 h, suggesting the particle size of the co-assembled nano-micelle increased, which might be due to protein adsorption after a long time of incubation. Though particle size of the co-assembled nano-micelles slightly increased, there were no aggregation or precipitation observed in the test duration, which implied the co-assemble nano-micelles may be suited for intravenous administration and targeted drug delivery.

3.3. In vitro drug release

It is anticipated that co-assembled nano-micelles could disassemble and realize controlled tumor intracellular drug delivery under high redox condition (2–10 mM GSH) of intra tumor cells. Treatment the prodrug molecules with DTT induces cleavage of the built-in disulfide bridge and two subsequent intramolecular cyclization reactions, one to cleave the urethane linkage to release the native GEM and the other to cleave the carbonate linkage to release the native CPT with 1,3-oxathiolan-2-one as the same byproduct [43] as depicted Scheme 2. In order to verify this potency, DTT-triggered *in vitro* drug release was evaluated. The drug release profile as a function of time is illustrated in Fig. 3. As depicted, in the period of 10 h, drug release of native CPT and GEM from co-assembled nano-micelles is lower than 20% at pH 7.4 with 20 μM DTT, the pH and reduction condition corresponding to the circumstances of blood circulation and extracellular matrices. In contrary, co-assembled nano-micelles exhibit significant rapid drug release at pH 6.5 with 2 mM DTT, the pH and reduction condition corresponding to that of tumor intracellular fluids. Under this condition, 100% of native CPT and GEM released within a period of 10 h. Meanwhile, in the same period of 10 h, cumulative release of CPT and GEM reach up to higher than 90% at pH 5.0 with 2 mM DTT, the pH and reduction condition corresponding to that of tumor intracellular endo/lysosome. Additionally, we also conducted the drug release at pH 5.0 and 6.5 with 20 μM DTT, the pH corresponding to that of tumor intracellular fluids or endo/lysosome, respectively and the reduction condition of blood circulation and extracellular matrices. As exhibited in Fig. S18, compared with higher DTT concentration (2 mM) corresponding to that of intra cellular compartments, the drug release was greatly decelerated with lower DTT concentration (20 μM, corresponding to that of extracellular fluids or blood plasma). In summary, in high redox environment, both pH 6.5 and pH 5.0 with 2 mM DTT, co-assembled nano-micelles show rapid drug release, which is supposed to realize prominent antiproliferative efficacy. Taken the results together, it implies that co-assembled nano-micelles, as expected, could minimize premature drug release in blood circulation while response to high redox condition of tumor cells to achieve redox-controlled rapid intratumor cells drug release.

3.4. In vitro cellular internalization

Previous studies have reported that PBA derivatives could facilitate tumor-targeting drug delivery through specific interaction with sialic acid epitopes overexpressed on tumor cells at physiological pH [21]. In order to verify the sialic acid-mediated specific endocytosis of the CPBA decorated co-assembled nano-micelles, *in vitro* cellular internalization was evaluated by fluorescence microscopy and RP-HPLC against MCF-7/ADR and 4T1 cells with SA overexpressed on cell surface [44,45].

As displayed in Fig. 4, after incubation for 24 h at 37 °C, the weak fluorescence of CPT demonstrated the low cellular internalization of free CPT and cocktail mixture of CPT and GEM against MCF-7/ADR cells. The observations may be resulted from the overexpression of reflux transporters in MCF-7/ADR cells. Overexpressed drug reflux transporters hamper the diffusion of free drugs into cells. In sharp contrast, bright blue fluorescence is visible for cells treated with CPBA decorated co-assembled nano-micelles. For further verify the role of CPBA-sialic acid interaction in cellular internalization, cells were pretreated with 5 mM CPBA for 30 min to block SA residues on cell surface. Before the competitive assay of *in vitro* cellular internalization, control cytotoxicity studies of both 5 mM CPBA pretreatment + CPT and 5 mM CPBA were carried out. As presented in Fig. S20, pretreatment with 5 mM CPBA for 30 min did not show significant cytotoxicity against MCF-7/ADR cells, the cell viability exceeded 90%. As exhibited in Fig. 4, pretreatment of cells with CPBA significantly diminish cellular internalization of the CPBA decorated co-assembled nano-micelles in MCF-7/ADR cells. However, the cellular uptake amount of CPBA pretreated group was lower than that of group treated by free CPT. It was thought that the decreased uptake was attributed to the slightly increased cytotoxicity and cell death induced by CPBA pretreatment + free CPT compared with free CPT alone as shown in Fig. S19 and Fig. 8. The dead cells were easily removed by washing with PBS resulted from the loss of adherence ability to the surface of culture plate, thereby resulted in the decreased cellular uptake. Overall, these results imply that the CPBA decorated co-assembled nano-micelles could remarkably facilitate cellular internalization through specific interaction with SA on surface of cancer cells.

In addition, RP-HPLC analysis was conducted for further quantitative evaluation of cellular internalization. As presented in Fig. 5, the results are in consistence with fluorescence microscopy observations.

Meanwhile, cellular internalization was evaluated against 4T1 cells. As presented in Fig. S11, the results are similar as that against MCF-7/ADR cells. Compared with free CPT and cocktail mixture of CPT and GEM, the CPBA decorated co-assembled nano-micelles show much higher cellular internalization. At the same time, cellular internalization greatly decreased against cells pretreated with free CPBA.

In order to elucidate whether cellular internalization of co-assembled nano-micelles is energy-dependent or not, cellular internalization was conducted under at 4 °C or 37 °C. As presented in Fig. 6A and Fig. 6B, in 4 h incubation period at 4 °C, cellular internalization of co-assembled nano-micelles is greatly impaired whereas cellular uptake proceeded successfully at 37 °C. In summary, the results demonstrate that cellular internalization of co-assembled nano-micelles is energy-dependent.

3.5. Drug accumulation and reflux

It has been widely reported in previous studies that nano-micelles could elude drug reflux and facilitate drug accumulation in multidrug resistant cell lines [46,47]. In order to verify the CPBA decorated co-assembled nano-micelles hold this merit, drug accumulation and reflux

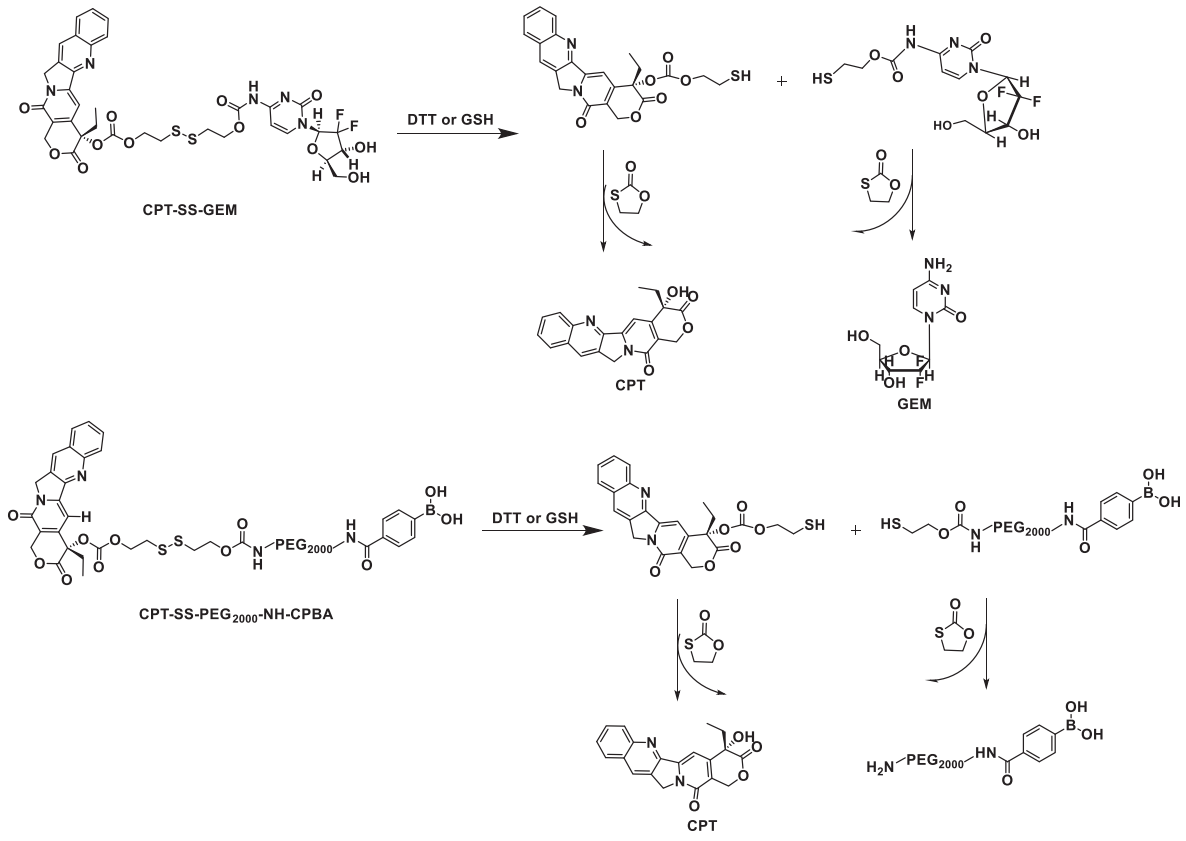

Scheme 2. Mechanism of reduction-triggered drug release.

investigation was performed against MCF-7/ADR and 4T1 cells. As exhibited in Fig. 7A, for MCF-7/ADR cells, the CPBA decorated co-assembled nano-micelles show ca. 1.5-fold higher drug accumulation than that of free CPT or cocktail mixture of CPT and GEM. Additionally, as displayed in Fig. 7C, it is noticeable that free CPT and cocktail mixture of CPT and GEM are largely pumped out from MCF-7/ADR cells in a time-dependent manner. Different from free CPT and cocktail mixture of CPT and GEM, the CPBA decorated co-assembled nano-micelles show minor drug efflux, which is about $\frac{1}{15}$ of free CPT and $\frac{1}{10}$ of cocktail mixture of CPT and GEM. It is speculated that these results may be mainly related to two reasons. On one hand, the CPBA decorated co-assembled nano-micelles could be internalized through endocytosis mediated by the specific interactions of CPBA and sialic acid thereby bypass drug efflux pumps. On the other hand, cleavage of disulfide bond of prodrugs involved in co-assembled nano-micelles is time- and reduction-dependent, which retard drug release and efflux. Furthermore, it demonstrates that cocktail mixture of CPT and GEM displays lower drug efflux than that of free CPT, which is consistent with the previous literature that multiple treatments could be reliable to overcome drug resistance [1]. It is worthy mentioned that for 4T1 cell line, the CPBA decorated co-assembled nano-micelles display much higher drug accumulation, nearly 2.2-fold of that against MCF-7/ADR cells. This result may be related to the higher overexpression of sialic acid on 4T1 cells than that on MCF-7/ADR cells. It is reported high sialic acid expression on cancer cell membrane is usual associated with tumor metastasis and 4T1 is a cancer cell line with high metastatic property

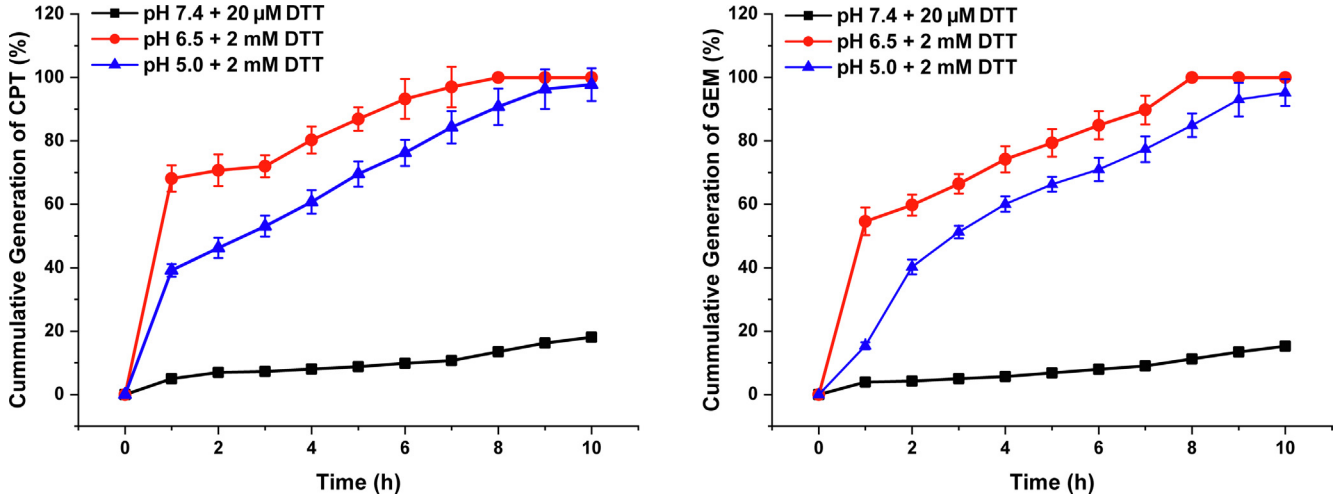

Fig. 3. Drug release profile of CPT and GEM from co-assembled nano-micelles in PBS at pH 7.4 with 20 μM DTT, pH at 6.5 or 5.0 with 2 mM DTT.

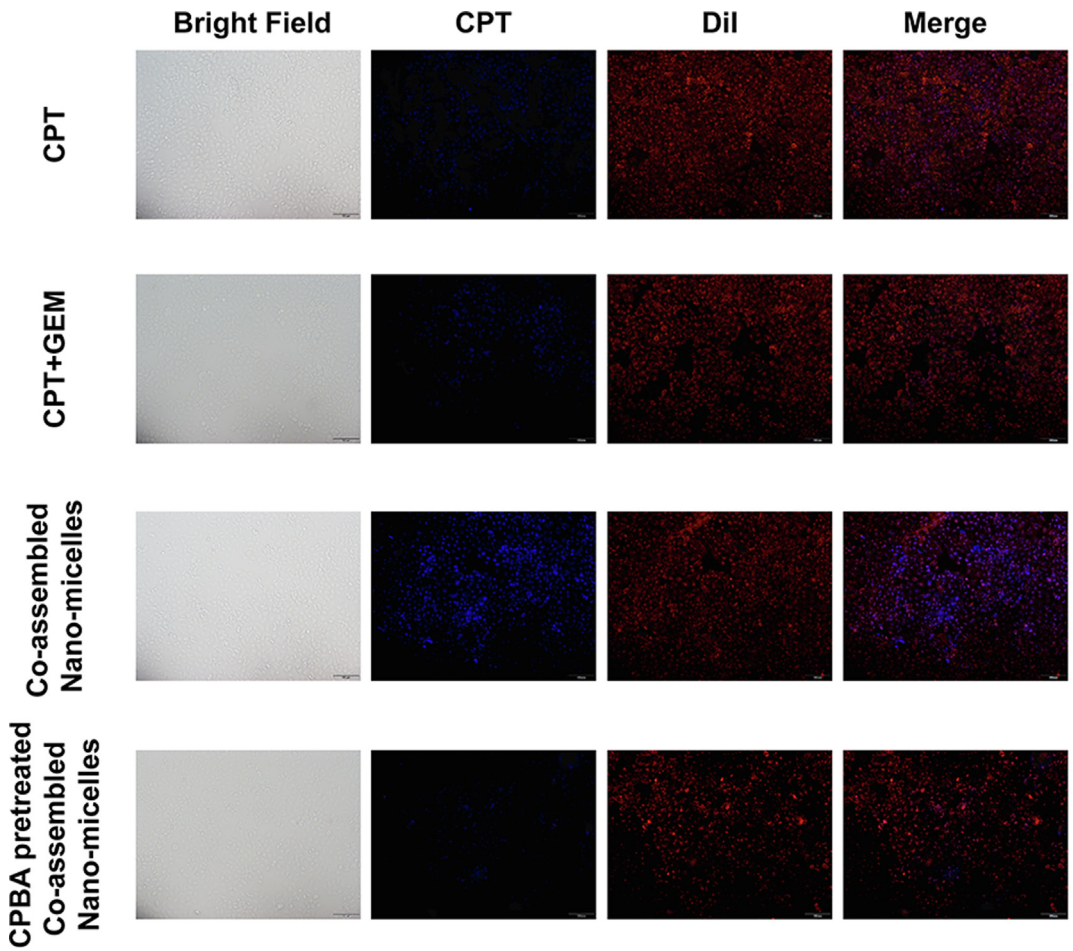

Fig. 4. Cellular internalization of CPT, GEM, cocktail mixture of CPT and GEM (molar ratio of CPT to GEM: 4/1) and co-assembled nano-micelles against MCF-7/ADR cells evaluated by fluorescence microscopy, scale bar: 100 μm.

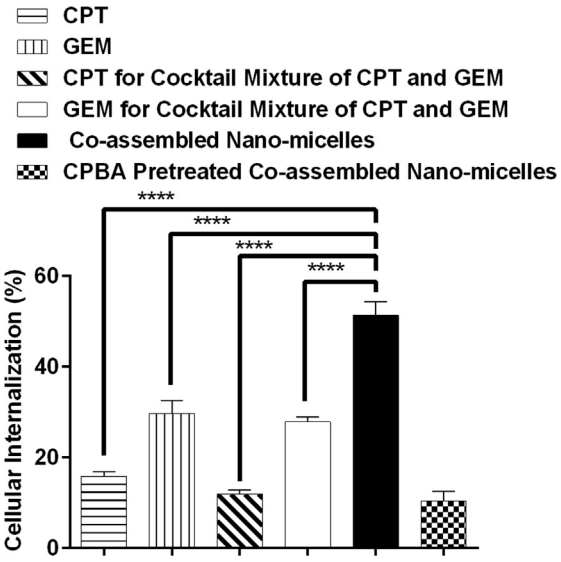

Fig. 5. Quantitative analysis of cellular internalization of CPT, GEM, cocktail mixture of CPT and GEM (molar ratio of CPT to GEM: 4/1) and co-assembled nano-micelles against MCF-7/ADR cells by RP-HPLC.

[48]. At the same time, compared with MCF-7/ADR cells, 4T1 cells exhibit not only higher drug accumulation but also lower drug efflux of free CPT, cocktail mixture of CPT and GEM and co-assembled nano-micelles, which probably due to the multidrug resistance of MCF-7/ADR.

3.6. *In vitro* cytotoxicity and multidrug resistance

It is widely acknowledged that overcoming multidrug resistance (MDR) is one of the virtues of drug combinations [5]. However, due to high expression of drug efflux pumps, such as p-glycoprotein (p-gp), various small molecular anticancer drugs could be pumped out from multidrug resistant cancer cells, which leads to decrement of intracellular drug accumulation far lower than the effective concentration [49]. Currently, due to the unique advantages, such as circumvent p-gp efflux pumps, enhancement of drug accumulation in tumor cells or at tumor site, stimuli-responsive controlled intracellular drug release, simultaneous targeting delivery of different drugs [3], nanotechnology-based combinational drug delivery has emerged as a promising strategy to overcome MDR.

Being consisted of two chemotherapeutic drugs with different action mechanisms, the co-assembled nano-micelles are considered potential to retrograde MDR of tumor cells. To this end, *in vitro* cytotoxicity of free CPT, GEM, cocktail mixture of CPT and GEM and the co-assembled nano-micelles were evaluated against MCF-7/ADR cells by standard MTT assay. Drug concentration of all treatments is equal to molarity of free CPT.

Obviously, as demonstrated in Fig. 8, the results validate the ascendant anticancer efficacy of co-assembled nano-micelles against MCF-7/ADR. All the different formulations display rather low concentration-dependent antiproliferative effect (inhibition rate < 35%) at drug concentration lower than 50 μM due to the strong drug

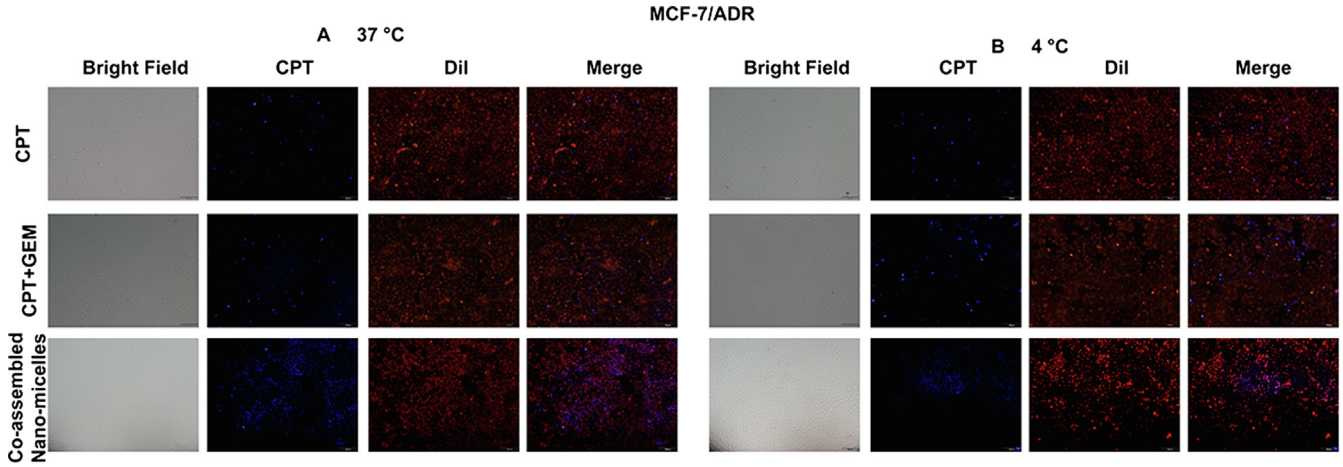

Fig. 6. (A) Cellular internalization of CPT, GEM, cocktail mixture of CPT and GEM (molar ratio of CPT to GEM: 4/1) and co-assembled nano-micelles at 37 °C for 4 h observed by fluorescence microscopy (B) Cellular internalization of CPT, GEM, cocktail mixture of CPT and GEM (molar ratio of CPT to GEM: 4/1) and co-assembled nano-micelles at 4 °C for 4 h observed by fluorescence microscopy.

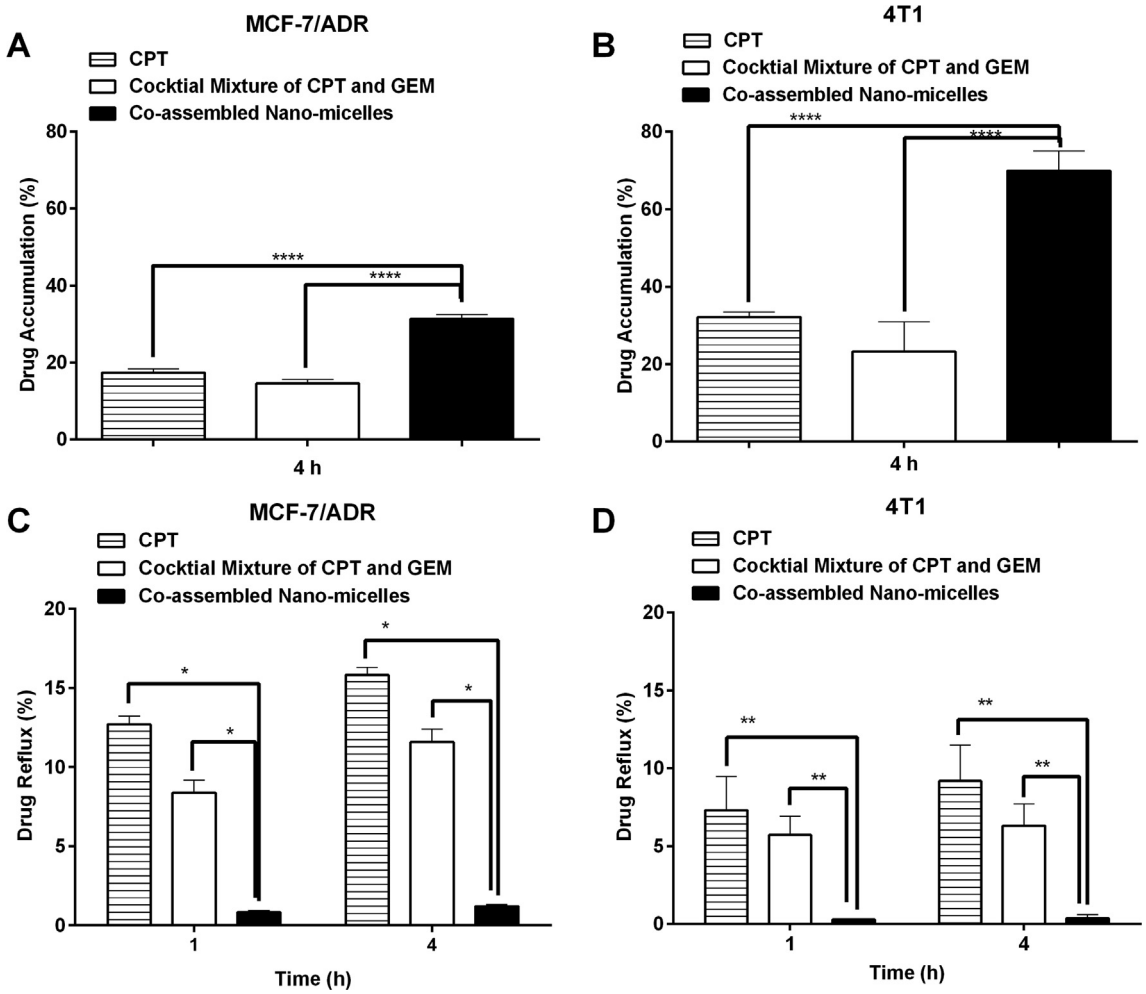

Fig. 7. Drug accumulation and reflux quantified by fluorescence spectrophotometer. (A), (B) Drug accumulation and (C), (D) drug efflux against MCF-7/ADR and 4T1 cells, respectively.

resistance of MCF-7/ADR cells. However, it's worth noting that at drug concentration of 50 μM, compared with other formulations, the cell viability treated by co-assembled nano-micelles remarkably decrease. It is speculated these results could be ascribed to the following reasons. Firstly, the co-assembled nano-micelles decorated with CPBA could bypass drug efflux pumps through endocytosis mediated by the specific interactions between CPBA and sialic acid as the results exhibited in Fig. 5, thereby greatly increase intracellular drug concentration. Secondly, it has previously reported that induction of multidrug resistance is associated with increased GSH level in tumor cells and GSH depletion

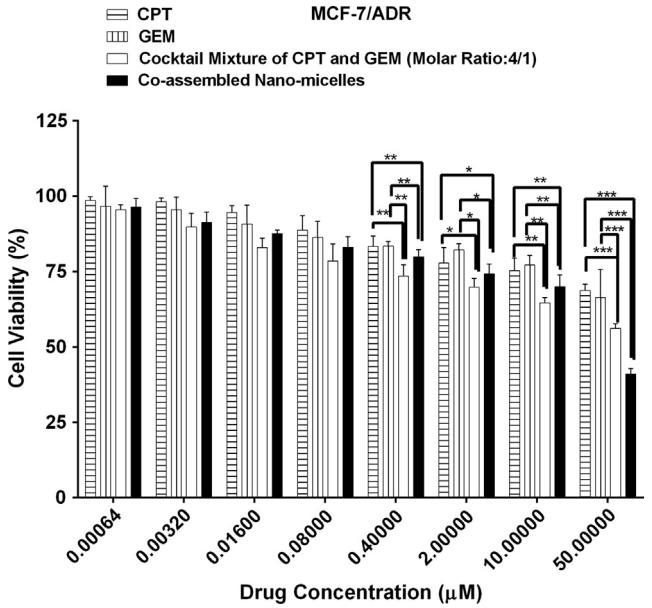

Fig. 8. *In vitro* cytotoxicity of different formulations against MCF-7/ADR cells for 72 h incubation determined by standard MTT assay. Data are expressed as mean ± SD (n = 3).

could sensitize tumor cells to therapy [50]. It is supposed that the cleavage of disulfide-bond in co-assembled nano-micelles consume intracellular GSH, which could contribute to inhibition of cancer cell proliferation. Furthermore, different from cocktail mixture of CPT and GEM, the redox-triggered disassembly and drug release of co-assembled nano-micelles facilitated ratio-metric synchronous intracellular delivery of CPT and GEM, which is benefit for antiproliferative efficacy. Collectively, the above-mentioned advantages of co-assembled nano-micelles greatly increase antiproliferative efficacy against MCF-7/ADR cells.

The IC_{50} values of all formulations were calculated and presented in Table S1. As presented, IC_{50} of co-assembled nano-micelles is much lower (30.59 ± 1.02 μM CPT and 7.65 ± 0.26 μM GEM) than that of free CPT (1047.13 ± 33.12 μM), free GEM (292.42 ± 6.69 μM) and cocktail mixture of CPT and GEM (249.46 ± 9.45 μM CPT and 62.37 ± 2.36 μM GEM). The IC_{50} of cocktail mixture of CPT and GEM is 4.20 fold lower than that of free CPT and 4.68 times lower than that of free GEM, which once again proves the synergism (CI for 50% inhibition rate is 0.562 ± 0.028) anticancer effect of the drug combination. Moreover, the IC_{50} of co-assembled nano-micelles is 8.15 times lower than that of cocktail mixture of CPT and GEM. In summary, these results demonstrate that the CPBA decorated co-assembled nano-micelles are potential in retarding drug resistance of MCF-7/ADR tumor cells.

In addition, cytotoxicity against 4T1 cell line was evaluated under different incubation period from 48 h to 96 h. As displayed in Fig. S12, it demonstrated that cell viability decreased with longer treatment period, especially for co-assembled nano-micelles. This result may be ascribed to drug release intra 4T1 cells is time- and redox- dependent. As presented, cocktail mixture and co-assembled nano-micelles exert superior antiproliferative efficacy compared with free CPT or free GEM at drug concentrations lower than 50 μM. The aforementioned results imply that drug combination is benefit for decrement of drug doses in cancer treatment due to synergism. What's more, all formulations exhibit superior antiproliferative efficacy against 4T1 cells compared with that of MCF-7/ADR cells. The IC_{50} of all treatments under different period were summarized in Tables S2–S4. IC_{50} value of free CPT and GEM show negligible time-dependent decrement, while that of cocktail mixture and co-assembled nano-micelles decrease greatly as increment of incubation period. In treatment period from 48 to 96 h, the IC_{50} value of co-assembled nano-micelles is higher than that of cocktail mixture, which may be related to the abovementioned time- and reduction-dependent intracellular drug release.

3.7. Determination of synergistic effect

Synergism is considered as the most important merit of drug combinations. In order to quantitatively evaluate the drug interaction nature and verify the synergism of cocktail mixture and co-assembled nano-micelles, combination index (CI) values were calculated by the Chou-Talalay equation using Calcusyn software. The nature of drug interactions are defined as antagonism with CI > 1.3, moderate antagonism with 1.1 < CI < 1.3, additivity with 0.9 < CI < 1.1, slight synergism with 0.8 < CI < 0.9, moderate synergism with 0.6 < CI < 0.8, synergism with 0.4 < CI < 0.6, and strong synergism with CI < 0.4 [39]. It is widely acknowledged that the plot of CI value against drug effect level (Fa, e.g. inhibition rate of 50%) clearly show quantitative information about the nature and extent of drug interactions. In this research, the CI values of cocktail mixture and co-assembled nano-micelles against MCF-7/ADR and 4T1 cell lines are calculated based on Eq. (1). Strikingly, as presented in Fig. 9, during 72 h incubation against MCF-7/ADR, all CI values at each corresponding Fa values of co-assembled nano-micelles are lower than CI = 0.5, while CI values of cocktail mixture increase sharply and exceeds CI = 1. These results denote the synergistic effect of co-assembled nano-micelles is much more prominent than cocktail mixture against MCF-7/ADR cells. In addition, CI values against 4T1 cells with different incubation period are shown in Fig. S13. As presented, CI values of cocktail mixture and co-assembled nano-micelles decrease as increment of incubation period from 48 h to 96 h. As shown in Fig. S13 and Fig. S14, at 48 h, CI values of cocktail mixture exceed CI = 1 at Fa higher than 0.7 while those at each corresponding Fa at 72 and 96 h are below CI = 1, and CI values are much lower at 96 h. The results demonstrate that prolongation of treatment period against 4T1 cells is benefit for exertion of synergism of the drug combination. Noteworthy, though decrease as increment of treatment period, CI values of co-assembled nano-micelles are still higher than that of cocktail mixture. This may be related to the time- and redox-dependent drug release profile of co-assembled nano-micelles while cocktail mixture is easier to directly exert anticancer efficacy. The difference of CI values of co-assembled nano-micelles against MCF-7/ADR and 4T1 cell lines may be ascribed to the heterogeneity of different cancer cell lines.

Additionally, reducing dosage of single drug used alone while

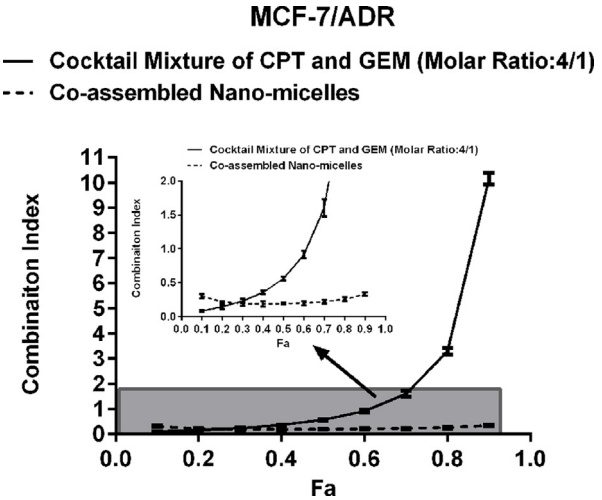

Fig. 9. Combination index of cocktail mixture of CPT and GEM, and co-assembled nano-micelles against MCF-7/ADR cells for 72 h incubation.

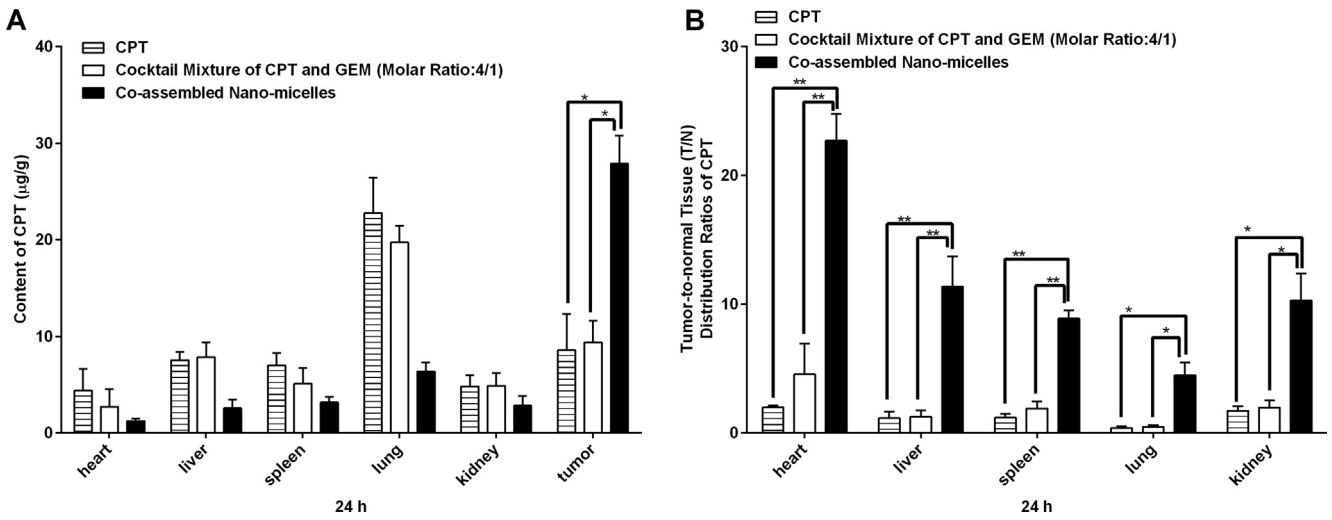

Fig. 10. Biodistribution of CPT, cocktail mixture of CPT and GEM, or co-assembled nano-micelles (drug concentration equivalent to 5 mg CPT/kg body weight) in mice burden 4T1 tumor after intravenous administration at 24 h. (A) Quantitative evaluation of *in vivo* biodistribution of different formulations in tumors and main organs normalized with organ or tumor weights. (B) Tumor-to-normal tissue distribution ratios for different formulations.

retaining its antiproliferative efficacy is another primary objective of synergistic drug combination. The DRI value, put forward by Chou JH and Chou TC [39], give quantitative information of dose-reduction in a synergistic combination at a given Fa value compared with single drug used alone. As displayed in Fig. S15, co-assembled nano-micelles show higher DRI values than that of cocktail mixture with 72 h treatment, especially at Fa higher than 0.2. At inhibition rate of 50%, DRI values of CPT and GEM in co-assembled nano-micelles are 7.05 ± 0.83 and 20.00 ± 1.28, respectively, which are almost 2.93 times of those in cocktail mixture, 2.41 ± 0.10 and 6.83 ± 0.59, respectively. Furthermore, as shown in Fig. S16, different from that against MCF-7/ADR cells, co-assembled nano-micelles display time-dependent increased but lower DRI values than that of cocktail mixture against 4T1 cells. For 96 h incubation, at inhibition rate of 50%, DRI values of CPT and GEM in co-assembled nano-micelles are calculated as 3.11 ± 0.22 and 9.07 ± 0.54, respectively whereas those in cocktail mixture are 7.57 ± 0.61 and 22.07 ± 1.41, respectively. In a word, co-assembled nano-micelles could greatly reduce drug dosage while retaining effective anticancer efficacy of free drugs used alone.

3.8. *In vivo* biodistribution

In vivo biodistribution of different formulations were evaluated against female BABL/c-nu mice bearing 4T1 tumors. After intravenous injection of free CPT, free GEM, cocktail mixture of CPT and GEM, and co-assembled nano-micelles for 24 h, the tumor-burden mice were euthanized. Then the main organs (heart, liver, spleen, lung and kidney) and tumor were collected for quantitative determination of drug distribution by fluorescence measurements. As presented in Fig. 10, after administration for 24 h, free CPT shows rather low accumulation at tumor site, which is similar as that of the cocktail mixture. It demonstrates that free CPT mainly accumulates in lung and liver. In contrast, the CPBA decorated co-assembled nano-micelles enhance drug accumulation at tumor site, which is about 2.5 folds of free CPT and cocktail mixture. Meanwhile, compared with free CPT or cocktail mixture, co-assembled nano-micelles decrease drug accumulation in normal tissues. Collectively, all the results demonstrate that the CPBA decorated co-assembled nano-micelles could reinforce the selective accumulation of drugs at tumor site.

4. Conclusions

In summary, the redox-sensitive CPBA-decorated rod-shaped nano-micelles with enhanced colloidal stability and increased absolute drug concentration are fabricated through a simple co-assembling strategy. Unlike cocktail mixture of free drugs, the nano-micelles could enable synchronous and ratio-metric delivery of CPT and GEM. Furthermore, the nano-micelles not only remarkably enhance cellular internalization *via* the CPBA-sialic acid interaction but also greatly decrease drug reflux by cancer cells. The cytotoxicity evaluation and quantitative calculation of CI and DRI values verify the prominent synergistic anticancer effect of the nano-micelles, which is potential for increment of treatment efficacy and decrement of dose-limiting toxicity. More important, the nano-micelles could both reinforce drug accumulation at tumor site and decrease that in normal tissues *in vivo*. Additionally, *in vivo* antitumor efficacy will be further evaluated through adjusting drug ratio to achieve optimal synergistic effect against different tumor models. Overall, the simple co-assembling tactic achieves the active targeting synergistic combinational delivery of CPT and GEM, and it may provide a potential platform for highly efficient combinational delivery of chemotherapeutics to exert profound therapeutic effect.

Declaration of Competing Interest

None.

Acknowledgements

The research work was supported by the National Natural Science Foundation of China [grant number 51573050, 81871405].

Appendix A. Supplementary material

Supplementary data to this article can be found online at https://doi.org/10.1016/j.ejpb.2019.09.019.

References

[1] J.A. Kemp, M.S. Shim, C.Y. Heo, Y.J. Kwon, "Combo" nanomedicine: co-delivery of multi-modal therapeutics for efficient, targeted, and safe cancer therapy, Adv. Drug Deliv. Rev. 98 (2016) 3–18.
[2] L. Miao, S. Guo, C.M. Lin, Q. Liu, L. Huang, Nanoformulations for combination or cascade anticancer therapy, Adv. Drug Deliv. Rev. 115 (2017) 3–22.
[3] C.M. Hu, L. Zhang, Nanoparticle-based combination therapy toward overcoming drug resistance in cancer, Biochem. Pharmacol. 83 (2012) 1104–1111.
[4] R.X. Zhang, H.L. Wong, H.Y. Xue, J.Y. Eoh, X.Y. Wu, Nanomedicine of synergistic drug combinations for cancer therapy – strategies and perspectives, J. Control. Release 240 (2016) 489–503.

[5] P. Parhi, C. Mohanty, S.K. Sahoo, Nanotechnology-based combinational drug delivery: an emerging approach for cancer therapy, Drug Discov. Today 17 (2012) 1044–1052.
[6] S.Y. Qin, A.Q. Zhang, S.X. Cheng, L. Rong, X.Z. Zhang, Drug self-delivery systems for cancer therapy, Biomaterials 112 (2017) 234–247.
[7] Q. Mou, Y. Ma, X. Zhu, D. Yan, A small molecule nanodrug consisting of amphiphilic targeting ligand-chemotherapy drug conjugate for targeted cancer therapy, J. Control. Release 230 (2016) 34–44.
[8] P. Huang, D. Wang, Y. Su, W. Huang, Y. Zhou, D. Cui, X. Zhu, D. Yan, Combination of small molecule prodrug and nanodrug delivery: amphiphilic drug-drug conjugate for cancer therapy, J. Am. Chem. Soc. 136 (2014) 11748–11756.
[9] Y. Wang, P. Huang, M. Hu, W. Huang, X. Zhu, D. Yan, Self-delivery nanoparticles of amphiphilic methotrexate-gemcitabine prodrug for synergistic combination chemotherapy via effect of deoxyribonucleotide pools, Bioconjug. Chem. 27 (2016) 2722–2733.
[10] P. Huang, J. Ao, L. Zhou, Y. Su, W. Huang, X. Zhu, D. Yan, Facile approach to construct ternary cocktail nanoparticles for cancer combination therapy, Bioconjug. Chem. 27 (2016) 1564–1568.
[11] Y. Xu, Y. Huang, X. Zhang, W. Lu, J. Yu, S. Liu, Carrier-free Janus nano-prodrug based on camptothecin and gemcitabine: reduction-triggered drug release and synergistic in vitro antiproliferative effect in multiple cancer cells, Int. J. Pharm. 550 (2018) 45–56.
[12] S.S. Pinho, C.A. Reis, Glycosylation in cancer: mechanisms and clinical implications, Nat. Rev. Cancer 15 (2015) 540–555.
[13] P. Radhakrishnan, S. Dabelsteen, F.B. Madsen, C. Francavilla, K.L. Kopp, C. Steentoft, S.Y. Vakhrushev, J.V. Olsen, L. Hansen, E.P. Bennett, A. Woetmann, G. Yin, L. Chen, H. Song, M. Bak, R.A. Hlady, S.L. Peters, R. Opavsky, C. Thode, K. Qvortrup, K.T. Schjoldager, H. Clausen, M.A. Hollingsworth, H.H. Wandall, Immature truncated O-glycophenotype of cancer directly induces oncogenic features, Proc. Natl. Acad. Sci. U.S.A. 111 (2014) E4066–4075.
[14] F. Dall'olio, N. Malagolini, M. Chiricolo, Glycosylation in cancer, Carbohydr. Chem. (2011) 21–56.
[15] S. Itzkowitz, T. Kjeldsen, A. Friera, S.-I. Hakomori, U.-S. Yang, Y.S. Kim, Expression of Tn, sialosyl Tn, and T antigens in human pancreas, Gastroenterology 100 (1991) 1691–1700.
[16] S. Pinho, N.T. Marcos, B. Ferreira, A.S. Carvalho, M.J. Oliveira, F. Santos-Silva, A. Harduin-Lepers, C.A. Reis, Biological significance of cancer-associated sialyl-Tn antigen: modulation of malignant phenotype in gastric carcinoma cells, Cancer Lett. 249 (2007) 157–170.
[17] E.P.B. Nuno, T. Marcos, Joana Gomes, Ana Magalhaes, Catarina Gomes, Leonor David, Imran Dar, Charlotte Jeanneau, Shawn DeFrees, Dorrit Krustrup, Lotte K. Vogel, Elin H. Kure, Joy Burchell, Joyce TaylorPapadimitriou, Henrik Clausen, Ulla Mandel, Celso A. Reis, ST6GalNAc-I controls expression of sialyl-Tn antigen in gastrointestinal tissues, Front. Biosci. 3 (2011) 1443–1455.
[18] R. Sewell, M. Backstrom, M. Dalziel, S. Gschmeissner, H. Karlsson, T. Noll, J. Gatgens, H. Clausen, G.C. Hansson, J. Burchell, J. Taylor-Papadimitriou, The ST6GalNAc-I sialyltransferase localizes throughout the Golgi and is responsible for the synthesis of the tumor-associated sialyl-Tn O-glycan in human breast cancer, J. Biol. Chem. 281 (2006) 3586–3594.
[19] J.A. Ferreira, P.A. Videira, L. Lima, S. Pereira, M. Silva, M. Carrascal, P.F. Severino, E. Fernandes, A. Almeida, C. Costa, R. Vitorino, T. Amaro, M.J. Oliveira, C.A. Reis, F. Dall'Olio, F. Amado, L.L. Santos, Overexpression of tumour-associated carbohydrate antigen sialyl-Tn in advanced bladder tumours, Mol. Oncol. 7 (2013) 719–731.
[20] S. Ricardo, L. Marcos-Silva, D. Pereira, R. Pinto, R. Almeida, O. Soderberg, U. Mandel, H. Clausen, A. Felix, N. Lunet, L. David, Detection of glyco-mucin profiles improves specificity of MUC16 and MUC1 biomarkers in ovarian serous tumours, Mol. Oncol. 9 (2015) 503–512.
[21] S. Deshayes, H. Cabral, T. Ishii, Y. Miura, S. Kobayashi, T. Yamashita, A. Matsumoto, Y. Miyahara, N. Nishiyama, K. Kataoka, Phenylboronic acid-installed polymeric micelles for targeting sialylated epitopes in solid tumors, J. Am. Chem. Soc. 135 (2013) 15501–15507.
[22] J. Kim, Y.M. Lee, H. Kim, D. Park, J. Kim, W.J. Kim, Phenylboronic acid-sugar grafted polymer architecture as a dual stimuli-responsive gene carrier for targeted anti-angiogenic tumor therapy, Biomaterials 75 (2016) 102–111.
[23] J.-Y. Lee, S.-J. Chung, H.-J. Cho, D.-D. Kim, Phenylboronic acid-decorated chondroitin sulfate a-based theranostic nanoparticles for enhanced tumor targeting and penetration, Adv. Funct. Mater. 25 (2015) 3705–3717.
[24] H. Meng, S. Yang, Z. Li, T. Xia, J. Chen, Z. Ji, H. Zhang, X. Wang, S. Lin, C. Huang, Z.H. Zhou, J.I. Zink, A.E. Nel, Aspect ratio determines the quantity of mesoporous silica nanoparticle uptake by a small GTPase-dependent macropinocytosis mechanism, ACS Nano 5 (2011) 4434–4447.
[25] K. Yang, Y.Q. Ma, Computer simulation of the translocation of nanoparticles with different shapes across a lipid bilayer, Nat. Nanotechnol. 5 (2010) 579–583.
[26] V.P. Chauhan, Z. Popovic, O. Chen, J. Cui, D. Fukumura, M.G. Bawendi, R.K. Jain, Fluorescent nanorods and nanospheres for real-time in vivo probing of nanoparticle shape-dependent tumor penetration, Angew. Chem. Int. Ed. Engl. 50 (2011) 11417–11420.
[27] Z. Zhou, X. Ma, E. Jin, J. Tang, M. Sui, Y. Shen, E.A. Van Kirk, W.J. Murdoch, M. Radosz, Linear-dendritic drug conjugates forming long-circulating nanorods for cancer-drug delivery, Biomaterials 34 (2013) 5722–5735.
[28] J.H. Park, G. von Maltzahn, L. Zhang, M.P. Schwartz, E. Ruoslahti, S.N. Bhatia, M.J. Sailor, Magnetic iron oxide nanoworms for tumor targeting and imaging, Adv. Mater. 20 (2008) 1630–1635.
[29] F. Cui, J. Lin, Y. Li, Y. Li, H. Wu, F. Yu, M. Jia, X. Yang, S. Wu, L. Xie, S. Ye, F. Luo, Z. Hou, Bacillus-shape design of polymer based drug delivery systems with janus-faced function for synergistic targeted drug delivery and more effective cancer therapy, Mol. Pharm. 12 (2015) 1318–1327.
[30] T. Ramasamy, H.B. Ruttala, B. Gupta, B.K. Poudel, H.G. Choi, C.S. Yong, J.O. Kim, Smart chemistry-based nanosized drug delivery systems for systemic applications: a comprehensive review, J. Control. Release 258 (2017) 226–253.
[31] J.A.S. Go Saito, Kyung-Dall Lee, Drug delivery strategy utilizing conjugation via reversible disulfide linkages role and site of cellular reducing activities, Adv. Drug Deliv. Rev. 55 (2003) 199–215.
[32] J.L.C. Dean, P. Jones, Paula S. Samiec, Paul Sternberg Jr., Vino C. Mody Jr., Robyn L. Reed, Lou Ann S. Brown, Glutathione measurement in human plasma Evaluation of sample collection, storage and derivatization conditions for analysis of dansyl derivatives by HPLC, Clinica chimica acta 275 (1998) 175–184.
[33] H.I.P. John, A. Cook, N. Susan, Lype, Norman Friedman, William DeGraff, Angelo Russo, James B. Mitchell, Cellular Glutathione and thiol measurements form surgically resected human lung tumor and normal lung tissue, Cancer Res. 51 (1991) 4287–4294.
[34] W.D. Angelo Russo, Norman Friedman, James B. Mitchell, Selective modulation of glutathione levels in human normal versus tumor cells and subsequent different response to chemotherapy drugs, Cancer Res. 46 (1986) 2845–2848.
[35] J. Chen, M. Zhao, F. Feng, A. Sizovs, J. Wang, Tunable thioesters as "reduction" responsive functionality for traceless reversible protein PEGylation, J. Am. Chem. Soc. 135 (2013) 10938–10941.
[36] Z. Yang, J.H. Lee, H.M. Jeon, J.H. Han, N. Park, Y. He, H. Lee, K.S. Hong, C. Kang, J.S. Kim, Folate-based near-infrared fluorescent theranostic gemcitabine delivery, J. Am. Chem. Soc. 135 (2013) 11657–11662.
[37] L. Zhang, D. Duan, Y. Liu, C. Ge, X. Cui, J. Sun, J. Fang, Highly selective off-on fluorescent probe for imaging thioredoxin reductase in living cells, J. Am. Chem. Soc. 136 (2014) 226–233.
[38] Ö. Topel, B.A. Çakır, L. Budama, N. Hoda, Determination of critical micelle concentration of polybutadiene-block-poly(ethyleneoxide) diblock copolymer by fluorescence spectroscopy and dynamic light scattering, J. Mol. Liq. 177 (2013) 40–43.
[39] T.C. Chou, P. Talalay, Quantitative analysis of dose-effect relationships: the combined effects of multiple drugs or enzyme inhibitors, Adv. Enzyme Regul. 22 (1984) 27–55.
[40] M.G.W. Liang Zhao, Jessie L-S. Au, Evaluation of combination chemotherapy integration of nonlinear regression, curve shift, isobologram, and combination index analyses, Clin. Cancer Res. 10 (2004) 7994–8004.
[41] F.F. Igor Nabiev, Irina Kudelina, Yves Pommier, Francoise Charton, Jean-Francois Riou, Alain J.P. Alix, Michel Manfait, Spectroscopic and biochemical characterisation of self-aggregates formed by antitumor drugs of the camptothecin family, Biochem. Pharmacol. 55 (1998) 1163–1174.
[42] S.Y. Qin, M.Y. Peng, L. Rong, B. Li, S.B. Wang, S.X. Cheng, R.X. Zhuo, X.Z. Zhang, Self-defensive nano-assemblies from camptothecin-based antitumor drugs, Regen. Biomater. 2 (2015) 159–166.
[43] Y. Zhang, Q. Yin, J. Yen, J. Li, H. Ying, H. Wang, Y. Hua, E.J. Chaney, S.A. Boppart, J. Cheng, Non-invasive, real-time reporting drug release in vitro and in vivo, Chem. Commun. (Camb.) 51 (2015) 6948–6951.
[44] C.H.X.Y. Lin, L.L. Yue, X.M. Zhao, J.C. Liu, Differential expression of the α2,3-sialic acid residues in breast cancer is associated with metastatic potential, Oncol. Rep. 25 (2011) 1365–1371.
[45] X. Wang, X. Li, Y.N. Zeng, F. He, X.M. Yang, F. Guan, Enhanced expression of polysialic acid correlates with malignant phenotype in breast cancer cell lines and clinical tissue samples, Int. J. Mol. Med. 37 (2016) 197–206.
[46] Y.C. Yu Gao, Xiufeng Ji, Xinyu He, Qi Yin, Zhiwen Zhang, Jianlin Shi, Yaping Li, Controlled intracellular release of doxorubicin in multidrug-resistant cancer cells by tuning the shell-pore sizes of mesoporous silica nanoparticles, ACS Nano 5 (2011) 9788–9798.
[47] H. Yu, Z. Cui, P. Yu, C. Guo, B. Feng, T. Jiang, S. Wang, Q. Yin, D. Zhong, X. Yang, Z. Zhang, Y. Li, pH- and NIR light-responsive micelles with hyperthermia-triggered tumor penetration and cytoplasm drug release to reverse doxorubicin resistance in breast cancer, Adv. Funct. Mater. 25 (2015) 2489–2500.
[48] I. Hauselmann, L. Borsig, Altered tumor-cell glycosylation promotes metastasis, Front. Oncol. 4 (2014) 28.
[49] M.M. Gottesman, T. Fojo, S.E. Bates, Multidrug resistance in cancer: role of ATP-dependent transporters, Nat. Rev. Cancer 2 (2002) 48–58.
[50] N. Traverso, R. Ricciarelli, M. Nitti, B. Marengo, A.L. Furfaro, M.A. Pronzato, U.M. Marinari, C. Domenicotti, Role of glutathione in cancer progression and chemoresistance, Oxid. Med. Cell. Longev. 2013 (2013) 972913.